JOURNAL OF SOLID STATE CHEMISTRY **137,** 127–137 (1998)
ARTICLE NO. SC977737

Raman Spectra and Vibrational Analysis of $BaFe_{12}O_{19}$ Hexagonal Ferrite

J. Kreisel,* G. Lucazeau,† and H. Vincent*,[1]

*Laboratoire des Matériaux et du Génie Physique (CNRS UMR 5628), ENSPG-INPG, B.P. 46, 38402 St. Martin d'Hères Cedex, France, and †Laboratoire d'Electrochimie et de Physicochimie des Matériaux et des Interfaces (CNRS UMR 5631), ENSEEG-INPG, B.P. 75, 38402 St. Martin d'Hères Cedex, France

Received December 2, 1997; accepted December 9, 1997

This paper reports on the first Raman spectra of barium hexaferrite, $BaFe_{12}O_{19}$, as a member of the magnetoplumbite-type structure. The spectra, recorded from 150 to 1000 cm^{-1} at room and liquid nitrogen temperature, are analyzed on the basis of D_{6h} factor group selection rules. The iron atom on the bipyramidal site is discussed with regard to its particular dynamics. The distribution of normal modes in $BaFe_{12}O_{19}$ is examined on the basis of the Raman spectra of β-alumina and a series of ferrites. Emphasis has been put on the factors influencing the Raman frequencies, namely the value of the coordination number, the degree of connection of a coordinated group, and the mass effect.

I. INTRODUCTION

Barium hexaferrite, $BaFe_{12}O_{19}$, denoted BaM by Braun (1), has generated a large research effort over the past 40 years because of its relevance in technological applications such as permanent magnets, microwave devices, and recording media (2, 3).

Surprisingly, vibrational spectra of BaM are scarce and have become only in recent times the object of research for different purposes. Polarized far-infrared reflection spectra have been used to investigate the optical and dielectric properties (4, 5). Eremenko *et al.* (6) studied infrared (IR) reflection spectra of cooled BaM single crystals. Finally, FT-IR powder spectra have been reported recently (7). Marshall and Sokoloff presented the ab initio calculation of phonon (8) and magnon (9) dispersion curves in anticipation of a detailed analysis of the ferrimagnetic resonance relaxation. However, in these works the vibrational properties are not described with regard to the crystal structure in terms of the spinel block and chemical entities. To our knowledge, no Raman study of BaM or, more generally, of the magnetoplumbite-type structure has been reported.

[1]To whom correspondence should be addressed.

On the other hand, vibrational spectroscopy (IR and Raman) of the less complicated spinel type oxides and rare earth orthoferrites has been widely applied for structural and physical property analysis. As for IR studies of spinels, we can mention the early works of Waldron (10), Preudhomme and Tarte (11–13), and Onari (14). More recently, Lutz *et al.* (15) and Baraton *et al.* (20) discussed both IR and Raman spectra whereas McCarty and Boehme (16), Graves *et al.* (17), and Degiori *et al.* (18) presented a Raman study. The Raman spectra of rare earth orthoferrites have been discussed by Venugopalan *et al.* (21, 22) and Koshizuka and Ushioda (23). Finally, Lucazeau and collaborators presented an extensive study of β-alumina (26–28), which contains spinel structure blocks.

The aim of this work is to analyze accurately the vibrational spectra of BaM to study its complex lattice dynamics with special regard to the environment of the five different Fe sites. In particular, our study is motivated by the need to build a database with regard to further studies such as

(i) the characterization of BaM thin films prepared by a new MOCVD injection method, developed in our group (30, 33). Recent results show that polarized Raman spectra can be used to investigate the texture on epitaxial and in plane-oriented thin films of oxides (19, 24).

(ii) the study of the cationic distribution on the Fe sites in Ir–Co-substituted BaM monocrystals (31, 32) and thin films with regard to magnetic properties.

For clarity, we present here only the results for nonsubstituted BaM single crystals. The detailed study of substituted crystals and thin films will be treated in a subsequent publication.

Furthermore, for the first time we derive by two different methods the full irreducible representation for the optical and acoustic modes. There is still controversy about the symmetry of the vibrational modes in the literature (4–8).

To assign the Raman spectra of BaM, we study extensively the influence of coordinated groups in the Raman spectra of ferrites. Furthermore, already published results on

0022-4596/98 $25.00

β-alumina have been used for a complementary comparison, especially with regard to the mass effect.

Finally, special attention has been drawn to the dynamics of the iron ion on the trigonal site of *M* hexaferrites, which is still a matter of debate (8, 34–39). Marshall and Sokoloff (8) proposed a new scenario for the dynamics and in particular a soft-mode behavior of the lowest transverse optic frequency which is coupled with the displacement from the mirror plane of this bipyramidal trigonal site. The experimental verification of this prediction is possible by measuring IR and Raman spectra at various temperatures. This study is an attempt to answer these questions.

II. EXPERIMENTAL

A. Samples

Single crystals of $BaFe_{12}O_{19}$ were grown from a Na_2O flux in platinum crucibles heated to 1400°C and cooled at 2°C/h to 1000°C as previously explained (35, 36). The Na_2O/Fe_2O_3 molecular ratio was approximately 0.6. Hexagonal platelets up to 3 mm across and 0.5 mm thick were obtained. The chemical composition was determined by microprobe analysis and the qualtiy was assessed by X-ray measurements.

B. Raman Spectroscopy

In the Raman spectra, all the samples were single crystals naturally cleaved perpendicular to the *c* axis. Polarized Raman spectra of these single crystals were recorded with a Dilor *XY* multichannel spectrometer equipped with a microscope. For the analysis of low-frequency spectra a Coderg T800 single-channel triple-monochromator spectrometer was used. The 514.5-nm line of an Ar^+ ion laser was used as the excitation line. Experiments were conducted in micro-Raman; the light was focused to 1-μm^2 spot. All measurements performed under the microscope were recorded in a backscattering geometry, including polarized Raman measurements. The instrumental resolution was $2.8 \pm 0.2\ cm^{-1}$. The temperature measurements were performed at 80 and 300 K using a sample chamber where the chamber was cooled with liquid nitrogen for low temperatures. We have verified that laser powers up to 10 mW did not produce significant heating or damage the sample. Standard experiments were carried out using incident powers of about 5 mW.

III. STRUCTURE AND SELECTION RULES

A. Crystal Structure

The magnetoplumbite crystal structure of $BaFe_{12}O_{19}$ (space group $P6_3/mmc$), found in 1938 by Adelsköld (40), was first extensively studied by Braun (1) and refined by Townes *et al.* (41). The crystal structure of BaM consists of a close-packed stacking of oxygen or barium–oxygen layers, and the iron atoms are distributed within three kinds of octahedral sites, one tetrahedral site, and one bipyramid site (Fig. 1). The structure is usually described in terms of two structural blocks: the spinel block S, $(Fe_{11}O_{16})^+$, separated by $(BaFeO_3)^-$ layers (block R).

As already mentioned in the introduction some ambiguities remain about the actual structure and dynamic properties of iron atoms located in the trigonal site; an overview and more detailed discussion is given in refs 8, 35, and 36. Using X-ray diffraction at room temperature, Townes *et al.* (41) suggested that the ion in the trigonal site

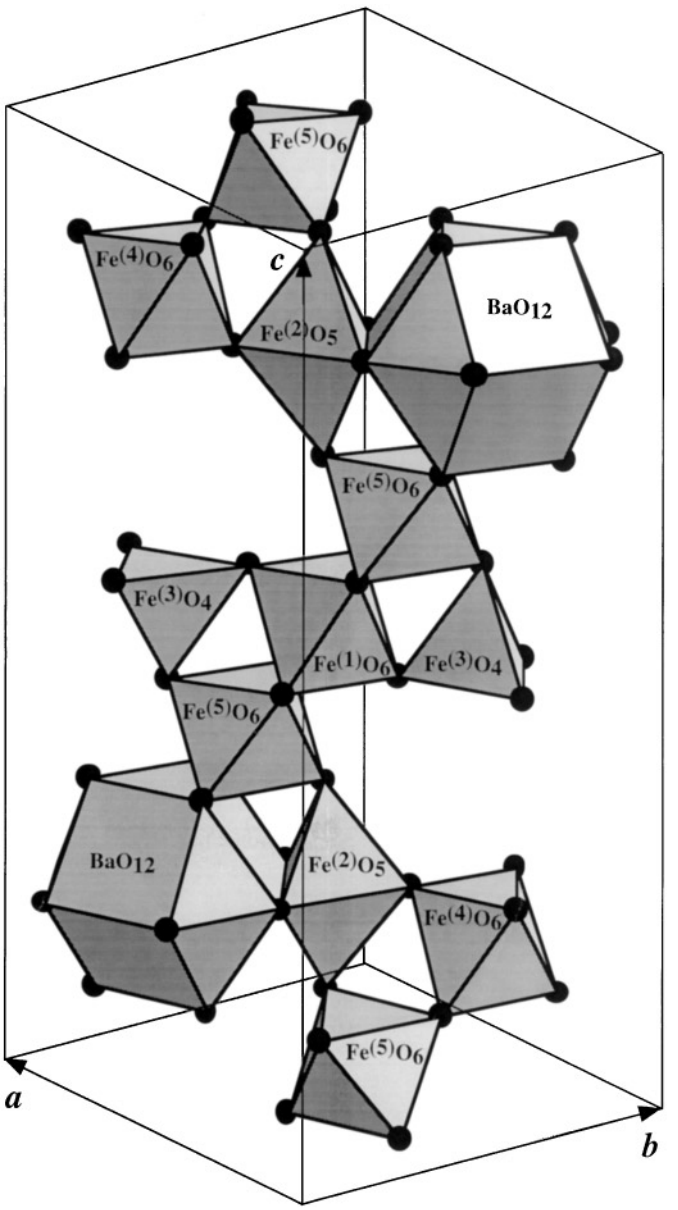

FIG. 1. Polyhedra of the $BaFe_{12}O_{19}$ crystal structure.

should be displaced some 0.156 Å from the 2*b* position in the mirror plane to the 4*e* position. A Mössbauer spectroscopy analysis reported by Rensen and Wieringen (34) confirmed these results. Kreber *et al.* (38, 39) again concluded a dynamic disorder at high temperature but proposed a static disorder below a transition temperature of 80 K. Obradors *et al.* (35, 36) deduced from X-ray analysis a dynamic disorder for the trigonal iron. Furthermore, Collomb *et al.* (37) performed a neutron diffraction experiment at 4.2 K and at room temperature and confirmed that at room temperature the iron atoms are displaced from the mirror plane, whereas at 4.2 K they observed a "frozen ion" in the mirror plane. More recently, Marshall and Sokoloff (8) proposed on the basis of their phonon spectral calculation a new hypothetical scenario for the temperature dependence of the trigonal site: At very low temperature the ion is located in a shallow minimum on the mirror plane. When the temperature approaches the critical value of 80 K, the mode softens; e.g., the frequency goes to zero. At a transition temperature of 80 K the authors assume a displacement to new equilibrium sites, what is now a very shallow double well, where the ions execute harmonic motions. In conclusion, the main difference between the more recent and older scenarios lies in the low-temperature region, where the ion is assumed to be located either in or out of the mirror plane.

B. Selection Rules

The 64 atoms in the unit cell give rise to 189 ($k = 0$) optical modes which can be characterized according to the D_{6h} factor group of the crystal by using group theoretical methods. As shown in Table 1 some discrepancies among previous works (4–8) can be observed. We decided to undertake a new detailed and complete analysis, also with respect to the characteristics of the bipyramidal site, which has been neglected up to now.

In a first step we used the correlation method reviewed by Fateley *et al.* (42). A main difficulty in this calculation lies in a correct choice for several site orientations; this point might be at the origin of faulty published results. From the correlation method, we can identify the species of the site group for each lattice vibration and correlate these species to the D_{6h} factor groups species. The total representation is then the sum of the individual irreducible representations.

TABLE 1

A. Crystal structure details, correlations used, and irreducible representation for BaM

Atom	Site			Site representation	Factor group representations											
	a	*b*	*c*		A_{1g}	A_{1u}	A_{2g}	A_{2u}	B_{1g}	B_{1u}	B_{2g}	B_{2u}	E_{1g}	E_{1u}	E_{2g}	E_{2u}
Ba	2*d*	D_{3h}	C_2''	$2A_2'' + 2E'$				1	1					1	1	
$Fe^{(1)}$	2*a*	D_{3d}	σ_d	$2A_{2u} + 2E_u$				1				1		1		1
$Fe^{(2)}$	2*b*	D_{3h}	C_2''	$2A_2'' + 2E'$				1	1					1	1	
$Fe^{(3)}$	4f_1	C_{3v}	σ_d	$4A_1 + 4E$	1			1	1			1	1	1	1	1
$Fe^{(4)}$	4f_2	C_{3v}	σ_d	$4A_1 + 4E$	1			1	1			1	1	1	1	1
$Fe^{(5)}$	12*k*	C_{1h}	σ_d	$24A_1' + 12A''$	2	1	1	2	2	1	1	2	3	3	3	3
$O^{(1)}$	4*e*	C_{3v}	σ_d	$4A_1 + 4E$	1			1	1			1	1	1	1	1
$O^{(2)}$	4*f*	C_{3v}	σ_d	$4A_1 + 4E$	1			1	1			1	1	1	1	1
$O^{(3)}$	6*h*	C_{2v}	C_2''	$6A_1 + 6B_1 + 6B_2$	1		1	1	1	1		1	1	2	2	1
$O^{(4)}$	12*k*	C_{1h}	σ_d	$24A' + 12A''$	2	1	1	2	2	1	1	2	3	3	3	3
$O^{(5)}$	12*k*	C_{1h}	σ_d	$24A' + 12A''$	2	1	1	2	2	1	1	2	3	3	3	3

B. Comparison of the irreducible representations given in the literature

Γ^d	11	3	4	14	13	4	3	12	14	18	17	15
$\Gamma^d_{\text{acoust.}}$				1						1		
$\Gamma^{d,e}_{\text{opt.}}$	11	3	4	13	13	4	3	12	14	17	17	15
Γ^f	13	4	3	14	10	5	5	10	18	20	13	13
$\Gamma^f_{\text{acoust.}}$				1						2		
$\Gamma^{f,g}_{\text{opt.}}$	13	4	3	13	10	5	5	10	18	18	13	13
$\Gamma^h_{\text{infrared}}$				14						17		

[a] Site occupied, Wyckoff notation.
[b] Site symmetry, Schoenflies symbol.
[c] Site elements used for the correlation between the site group and the factor group.
[d] Our results.
[e] Reference 6.
[f] Reference 4.
[g] Reference 7.
[h] Reference 8.

To test our results we used in a second step the Bhagavantam–Venkatarayudu technique (43); the results of both calculations are identical.

The results in Table 1A show that, based on D_{6h} symmetry, 42 Raman-active modes ($11A_{1g} + 14E_{1g} + 17E_{2g}$) and 30 IR-active modes ($13A_{2u} + 17E_{1u}$) are expected. The other optical modes are silent modes ($3A_{1u} + 4A_{2g} + 13B_{1g} + 4B_{1u} + 3B_{2g} + 12B_{2u} + 15E_{2u}$). One A_{2u} mode and one doubly degenerate E_{1u} mode correspond to acoustic modes. Table 1B presents the results in comparison with the literature.

In the foregoing derivation the iron $Fe^{(2)}$ was placed on the mirror plane. However, as already mentioned one must also consider the case where the $Fe^{(2)}$ equilibrium positions are displaced from the mirror plane to pseudotetrahedral $4e(C_{3v})$ sites. A static or (and) a dynamic disorder might be considered (8, 34–39).

Assuming a dynamic disorder, which from a spectroscopic point of view implies a jump frequency between split positions larger than $10^{13}\,s^{-1}$, the same selection rules can be conserved. As the temperature decreases, the hopping rate decreases and a complete ordering might take place and give rise to a superstructure. For the case of a superstructure, the total number of bands is expected to increase considerably. Note that when the atom changes its position via tunneling (at low temperature), band splitting can be expected. This discussion will be continued in Section V.B.1.

IV. RESULTS

The frequencies of the Raman bands observed at room temperature and 80 K are listed along with the appropriate symmetry assignments in Table 2. Representative

TABLE 2
Assignment of the BaM Raman Spectra

Frequency (cm^{-1})		Raman tensors[a]				Assignments	
300 K	80 K	$X(YZ)\bar{X}$	$X(ZZ)\bar{X}$	$Z(XY)\bar{Z}$	$Z(YY)\bar{Z}$	[b]	Description
173	176	7	1	1		E_{1g}	Whole spinel block
184	187	18	2	2		E_{1g}	Whole spinel block
208	212			3	4	E_{2g}	
212	216	4				E_{1g}	
215	218	3				E_{1g}	
216	220		10			A_{1g}	O–Fe–O bridge
250	251	3				E_{1g}	
285	287	5				E_{1g}	
317	319		10		5	A_{1g}	
319	323			3	5	E_{2g}	
317	322	8				E_{1g}	
335	340			11	13	E_{2g}	
340	346		13			A_{1g}	Octahedra (mixed)
340	346	7				E_{1g}	
385	388			3	4	E_{2g}	
409	413		14		5	A_{1g}	$Fe^{(5)}O_6$ octahedra dominated
417	416	4				E_{1g}	
420	422			4	5	E_{2g}	
451	452	4				E_{1g}	
453	462		10			A_{1g}	
467	473		16		4	A_{1g}	Octahedra $Fe^{(1)}O_6$ and $Fe^{(5)}O_6$
512	513		11		2	A_{1g}	
–	516					E_{2g}	
527	530	4				E_{1g}	
529	533			7	9	E_{2g}	
566	574			3	4	E_{2g}	
606	607	3		2		E_{2g}	
609	611			1		E_{1g}	
611	612	1				E_{1g}	Octahedra (mixed)
612	613			2		E_{2g}	
614	620		26		11	A_{1g}	Octahedra $Fe^{(4)}O_6$
684	688	4	49	3	40	A_{1g}	Bipyramid $Fe^{(2)}O_5$
713	722	1	16	1	13	A_{1g}	Tetrahedra $Fe^{(3)}O_4$

[a] 300 K spectra.
[b] Symmetry assignment based on the analysis of the observed Raman tensors.

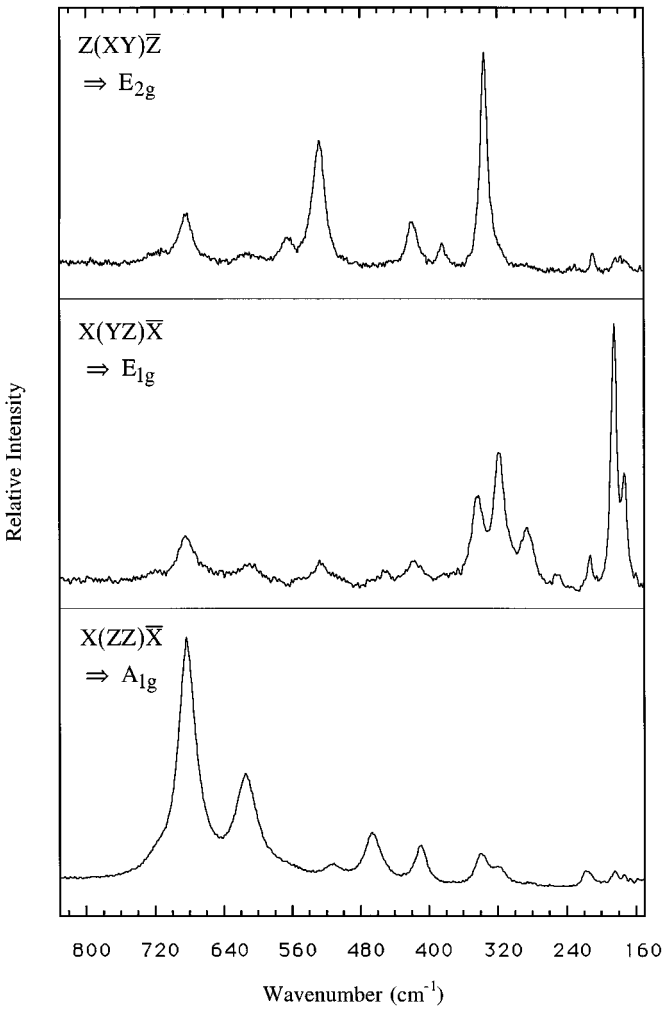

FIG. 2. BaM Raman spectra recorded at 300 K.

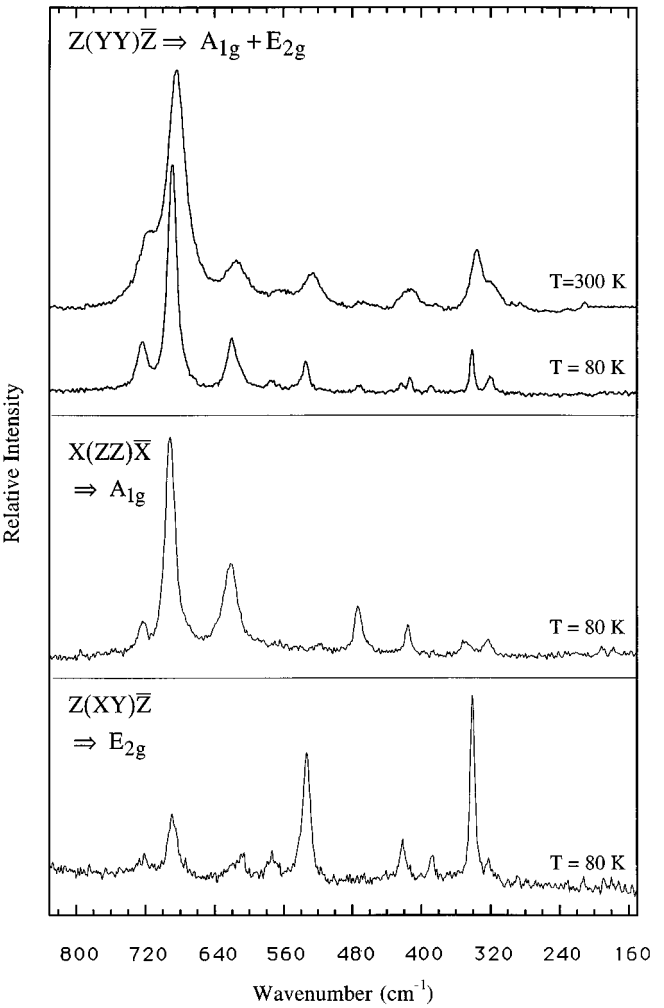

FIG. 3. BaM Raman spectra recorded at 80 K in comparison to a 300 K spectrum.

single-crystal spectra for several scattering geometries are shown in Fig. 2. Figure 3 shows, for comparison, a selection of the observed low-temperature spectra.

All the obtained Raman spectra show a marked polarization effect, which indicates a good orientation and a good crystal quality. The symmetry assignments in Table 2 are based on the analysis of Raman tensors measured by polarization analysis. The $X(ZZ)\bar{X}$ and $Z(XY)\bar{Z}$ spectra were useful to distinguish A_{1g} from E_{2g} modes, since both of these modes appear in the $X(YY)\bar{X}$ and $Z(XX)\bar{Z}$ configurations. In this way the bands characterized by a drastic enhancement or even disappearance in the $Z(XY)\bar{Z}$ spectrum can be identified as A_{1g} modes. The same argumentation is used to identify the doubly degenerate E_{2g} modes. The E_{1g} modes are similarly obtained from the $X(YZ)\bar{X}$ spectra. Nevertheless, some components appear in more than one spectrum. Due to the strong polarization effect observed for the other lines, they have been considered as distinct lines. Thus, we have identified 10 (11 expected) A_{1g}, 13 (14) E_{1g}, and 10 (17) E_{2g} modes. The absence of lines, especially for the off-diagonal polarization, might be among others due to nondetectable lines below 150 cm^{-1}. We tried to investigate the low-frequency region with a Coderg T800 single-channel spectrometer but no band could be detected due to the weak intensity of the BaM spectra.

V. DISCUSSION

A. Assignments Based on Ferrites and β-Alumina Vibrational Data

When only the shortest Fe–O bonds are considered, one can define the BaM crystal structure as made of FeO_4 tetrahedra, FeO_6 octahedra, and FeO_5 bipyramid and dodecacoordinated Ba^{2+} cations. The compound is made of the following structural units (35, 36) :

(i) Block S: The stacking of this S block along the *c* axis is the same as the well-known cubic spinel structure along the (111) cubic axis. The $Fe^{(5)}O_6$ octahedra share edges among

themselves and corners with the $Fe^{(3)}O_4$ tetrahedra, which is slightly axially compressed. In contrast to the $Fe^{(1)}O_6$ octahedron, which is regular (6×2 Å), the $Fe^{(5)}O_6$ octahedron is more distorted with point symmetry *m*.

(ii) Block R: The Ba site is 12-coordinated with two sets of Ba–O distances, leading to a slightly axially compressed polyhedron. In addition to the Ba polyhedron, $Fe^{(4)}$ cations form two octahedra sharing a face in the mirror plane. In this case the strong Fe^{3+}–Fe^{3+} electrostatic repulsion makes the octahedra more distorted. Finally, the R block contains the $Fe^{(2)}$ trigonal bipyramid site, a not very common coordination in ferrites. This bipyramid site can be regarded as two tetrahedra, axially compressed, sharing a face in the mirror plane.

The frequency distribution of the normal modes in ferrites may be expected to provide additional insight into the origin of the Fe–O dominated modes of BaM, on the other hand, the well-studied Na-β-alumina (Na-β), which also contains spinel blocks, crystallizes, in a quite similar crystal structure and is therefore an excellent reference.

For ionic materials such as the oxides of Fe^{3+}, both IR- and Raman-active modes are lattice vibrations involving the participation of all the atoms. This makes it difficult to propose an empirical assignment of the experimental bands to a particular vibrational mode of the basic structure units of the solid. In such cases, simplified methods must be used (11). It is actually well known that, apart from the chemical nature and the valency state of the cation *A*, the value of the coordination number *n* is the principal factor determining the vibrational frequencies of a coordinated group AO_n: the smaller the coordination number, the shorter the bond length and hence the higher the vibration frequencies. For a better understanding of the following discussion, the reader should consider Fig. 4.

1. Na-β-alumina. The differences between the BaM and the ideal β-alumina crystal structure lie in the mirror plane of the block R: In the mirror plane of BaM an additional trivalent iron atom, $Fe^{(2)}$, is located in a trigonal bipyramidal site, in contrast to the β-alumina structure, where this atom is missing. Moreover, a triangle of three oxygen atoms in the magnetoplumbite structure is replaced in the alumina structure by an oxygen located at the center of mass of the triangle. Only 38 vibrational modes, instead of 42 for BaM, are expected in the Raman spectrum ($10A_{1g} + 13E_{1g} + 15E_{2g}$) (29). A general review of the static and dynamic structure of β-alumina is presented in ref 27. A comparison of the Raman spectra (see Fig. 4.I) is interesting in view of the characterization of bands associated with the bipyramidal $Fe^{(2)}O_5$ polyhedra and more generally of the mass effect for bands associated with spinel block vibrations.

The main difficulty in a study of the mass effect in isostructural compounds is the knowledge of the effective masses to be taken into consideration. In other words, the frequency ratio for a given vibration in a specific MO_n group will vary from 1 to $(\mu_M/\mu_{M'})^{1/2}$ (where μ is the reduced mass) and $(M/M')^{1/2}$ depending on which content metals are allowed to move. Dohy *et al.* (28) presented a description of the normal modes of Na-β in terms of the largest atomic displacements and localized vibrations. In this way they were able to propose an assignment of the modes based on the dominant participating atoms. The use of this information allows one to correlate nearly all the BaM and Na-β frequencies of A_{1g} symmetry and so interpret approximately the BaM spectra in terms of contributing atoms. Figure 4.II.a shows on the right side the mass ratio for different types of atomic motions. On the left side we present a simplified interpretation which might be adopted for the frequency ratio of BaM and Na-β (see Fig. 4.II.b) for a given mode. The assignment based on these considerations is given in Table 2. The foregoing discussion has only been done for the A_{1g} modes because of the lack of spectral data for the E_{1g} and E_{2g} modes.

2. Ferrites. A comparison of the IR spectra of inorganic aluminates can be made on the assumption, proposed by Tarte (11), that tetrahedral and octahedral groups absorb at different frequencies in the IR spectra. Tarte also concluded that "condensed" polyhedra absorb at higher frequencies than the corresponding "isolated" polyhedra.

Because of a lack of data a systematic comparison is less easy for Raman spectra of ferrites, and, to our knowledge, it has never been done. Therefore we will try to use this simple "molecular" approach by using Raman spectra of known ferrites.

FeO_4 tetrahedra. This type of arrangement is found for γ-Fe_2O_3 (maghemite) and for inverse II–III spinels such as $MgFe_2O_4$, $NiFe_2O_4$, and magnetite (Fe_3O_4). For comparison with BaM the schematic spectra of these compounds are shown in Fig. 4.III. The general formula for a spinel is AB_2O_4. *A* refers to an M^{2+} ion and *B* refers to an M^{3+} ion. In the inverse spinel structure the trivalent cation occupies all the tetrahedral sites whereas the octahedral sites are filled half by the bivalent cation and half by the trivalent cation. A symmetry-based normal mode assignment for cubic spinels was first given by White and DeAngelis (44): four IR-allowed ($4F_{1u}$) and five Raman-allowed ($A_{1g} + E_g + 3T_{2g}$) lattice modes were predicted. Graves *et al.* (17) suggested a new irreducible representation based on a symmetry brought about by lattice defects which leads to a splitting of one T_{2g} mode into $A_{1g} + E_g$ representations. However, such a splitting was not observed for Fe_3O_4 by other authors (18, 46). Thus the 706-cm^{-1} line reported for $NiFe_2O_4$ and Fe_3O_4 in ref 17 could be due to an impurity-related phonon and we concluded the irreducible representation of ref 41 and the data of ref 43. The individual

spectra of the inverse spinels discussed here are different but are characterized by a common feature, namely a strong A_{1g} band in the 670 to 710-cm^{-1} region (18, 43). This behavior is observed irrespective of the chemical nature of the bivalent cation; therefore these bands must be assigned to stretching vibrations of FeO_4 tetrahedra. Bands in this region can also be observed for γ-Fe_2O_3 (20), which also contains Fe^{3+} tetrahedra.

FeO_6 octahedra (*see Fig. 4.IV*). Hematite, α-Fe_2O_3, is the simplest case, since its structure contains FeO_6 octahedra only. A characteristic feature is the occurrence of the highest band at about 600 cm^{-1} of E_g symmetry and an A_{1g} mode at 498 cm^{-1} (16, 45). The spectra of the normal II–III spinels AFe_2O_4 (A = Zn, Mn) can also be taken as an example for a 6-coordinated iron, since the A ions occupy the tetrahedral sites and the iron ions occupy only octahedral sites. The normal II–III spinels exhibit a band of A_{1g} symmetry in the 600- to 620-cm^{-1} region (17, 47), in contrast to the inverse spinel, where no band is observed at higher frequency. As observed above, this behavior is observed irrespective of the chemical nature of the bivalent cation, so it may be assumed that this band is essentially an Fe–O vibration of the FeO_6 octahedron. Octahedral units are also present in rare earth orthoferrites $RFeO_3$ (R = Er, Tm, Tb, Dy, Ho), which are built of FeO_6 octahedra and RO_{12} dodecahedra only. Here again, one can observe common features (21–23): The band with A_g symmetry in the 480- to 520-cm^{-1} region must be assigned to stretching modes of the octahedra. According to Tarte (11), it is of importance to specify if the groups under consideration are "isolated" or "condensed"; the notation is not to be taken literally but instead refers to the degree of connection of the coordinated group. If we apply this notation, we find a lower degree of connection for the octahedra of orthoferrites than for normal spinels. As a consequence, the highest A_{1g} mode for the orthoferrites is located at lower frequency than observed for the spinels. It might be objected that one type of structure only (orthoferrite type) has been investigated here; however, the region 480–520 cm^{-1} seems to be representative of octahedra with a low degree of connection.

In conclusion, ferrites containing $Fe^{(3+)}O_4$ tetrahedra are characterized by Raman bands in the 660- to 720-cm^{-1} region, whereas A_{1g} modes observed in the 460- to 640-cm^{-1} region might be assigned to motions which are dominated by $Fe^{(3+)}O_6$ octahedra. Furthermore, the consideration of the degree of connection of the coordinated group might be a helpful tool for the Raman spectra assignment of such compounds. The authors are aware that one has to take care when using the above comparison, because the vibrational interactions between the groups may sometimes be so large that the concept of "separate" vibrations is meaningless. A complementary analysis, such as isomorphic (such as presented in this paper with Na-β) and isotopic replacement, is advised.

3. Comparison and Assignment. On the basis of the previous discussion we will try to apply these two complementary concepts to assign the Raman spectra of BaM.

In the Raman spectra of a-β one band of A_{1g} symmetry at high frequency (895 cm^{-1}) is separated by a region free of bands from the rest of the spectra. On the other hand, in the Raman spectra of BaM an A_{1g} doublet, composed of a weak band at high frequency (684 cm^{-1}) and a very strong band at 712 cm^{-1}, is observed. As already seen for Na-β, this doublet is separated by a region free of bands from the rest of the spectra. In the following, we will show that the weak A_{1g} band at 712 cm^{-1} corresponds to the motions of the tetrahedra, as in Na-β, and that the strong band at 684 cm^{-1} corresponds to a mode of the bipyramidal group, which does not exist in Na-β.

The arguments are the following: If we consider a frequency ratio of 1.25 for BaM and Na-β, as can be observed for the highest A_{1g} and E_g modes in isostructural α-Al_2O_3 (48) and α-Fe_2O_3 (45), this leads to 716 cm^{-1}. This is in excellent agreement with the mode observed a 713 cm^{-1} for BaM. Based on calculations this mode has been assigned (28) to an AlO_4-dominated motion. The strong band in the BaM spectrum, absent for Na-β, can be explained by considering the additional bipyramidal site in BaM, which can be seen as two tetrahedra. The $Fe^{(2)}O_5$ bipyramid has a higher coordination compared to the tetrahedra and is therefore assumed to be at lower frequency. It is useful to examine the modes expected from the group theory calculation for this bipyramid (Table 1). The $Fe^{(2)}$ atom in the center of the $Fe^{(2)}O_5$ bipyramid does not give rise to a mode of A_{1g} symmetry; therefore the A_{1g} vibrations of this unit are expected to be dominated by the oxygen atoms ($O^{(1)}$ and $O^{(3)}$). Bands due to such a vibration are known to be very intense, as can be observed for the mode at 684 cm^{-1}, which is the most intense band of the BaM spectra. Furthermore, there is an apparent correlation between the A_{1g} modes in the 670 to 710-cm^{-1} region (17, 18, 46) in AFe_2O_4 (A = Mg, Ni, Fe) and the bands of corresponding symmetry at 713 and 684 cm^{-1} in BaM. Following the argumentation stated for ferrites, bands found in this region might correspond to the stretching modes of tetrahedral units. This is in good agreement with the previous argumentation. In conclusion, the Raman mode at 684 cm^{-1} can be assigned to the motions of the $Fe^{(2)}O_5$ bipyramidal group and the mode at 713 cm^{-1} to the $Fe^{(3)}O_4$ tetrahedral group.

In the same way, for the 450- to 620-cm^{-1} region it is reasonable to compare the BaM spectra with the ferrite spectra dominated by octahedral groups. There is an obvious correspondence of the A_{1g} mode at about 615 cm^{-1} observed for AFe_2O_4 (A = Mn, Zn) and A_{1g} mode observed at 614 cm^{-1} for BaM, and it might therefore be assigned to the motion of an octahedron. Respecting the above argumentation that phonons of octahedra with a higher degree of connection are found at higher frequencies, the mode at

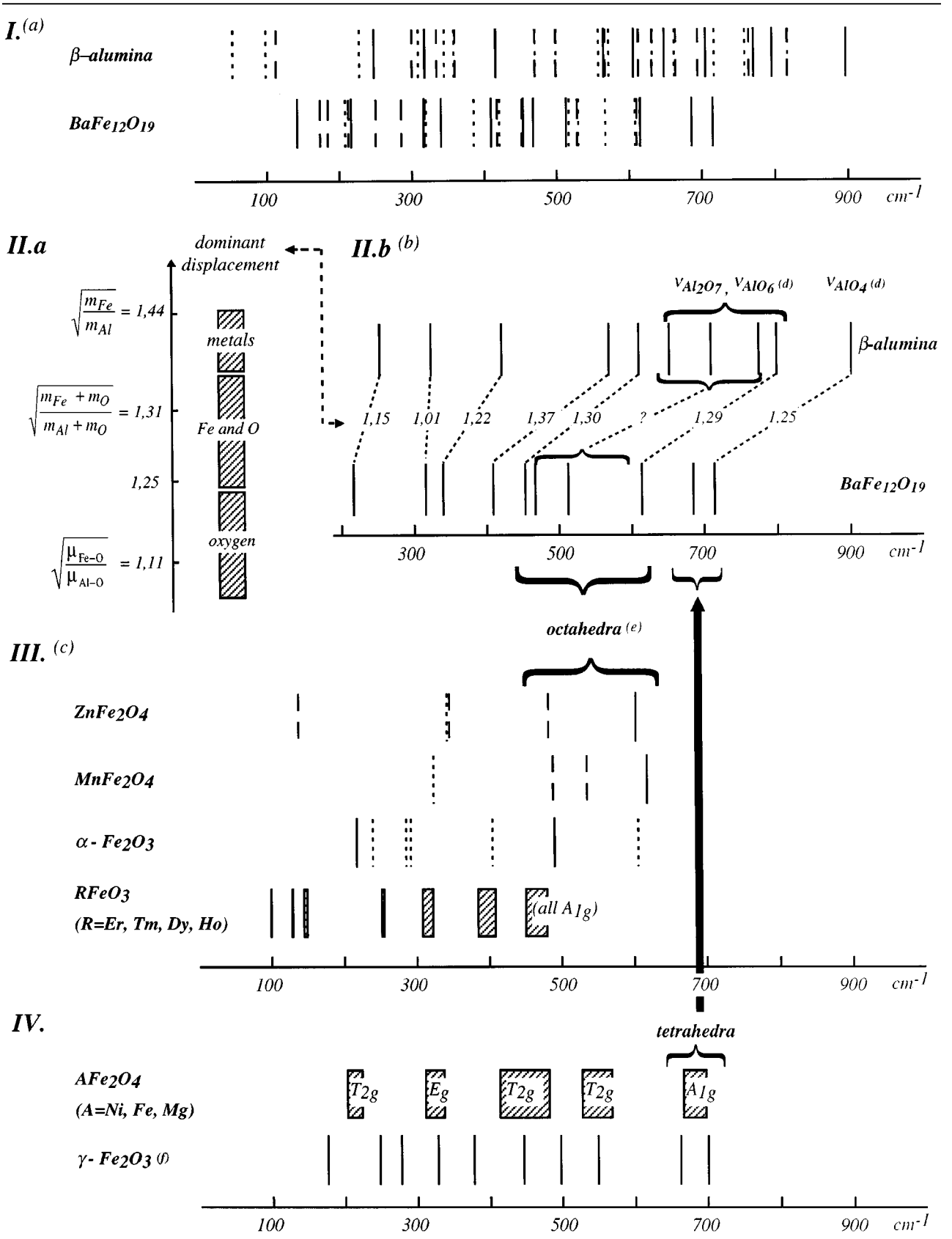
I.(a)
β–alumina
BaFe12O19
100
300
500
700
900
cm-1
II.a
dominant displacement
√(mFe/mAl) = 1,44
metals
√((mFe + mO)/(mAl + mO)) = 1,31
Fe and O
1,25
oxygen
√(μFe–O/μAl–O) = 1,11
II.b (b)
νAl2O7, νAlO6 (d)
νAlO4 (d)
β-alumina
1,15
1,01
1,22
1,37
1,30
?
1,29
1,25
BaFe12O19
300
500
700
900
cm-1
octahedra (e)
III. (c)
ZnFe2O4
MnFe2O4
α- Fe2O3
RFeO3
(R=Er, Tm, Dy, Ho)
(all A1g)
100
300
500
700
900
cm-1
IV.
tetrahedra
AFe2O4
(A=Ni, Fe, Mg)
T2g
Eg
T2g
T2g
A1g
γ- Fe2O3 (f)
100
300
500
700
900
cm-1

614 cm^{-1} should be assigned to the distorted $Fe^{(4)}O_6$ octahedra. There is a probable correlation between the A_{1g} phonon in α-Fe_2O_3 at 498 cm^{-1} and the observed one at 512 cm^{-1} for BaM. Furthermore, the A_{1g} modes at 512, 467, and 453 cm^{-1} in BaM fall in the region of octahedra motions observed for rare earth orthoferrites. A comparison with Na-β spectra using the mass ratio is not straightforward because of the missing experimental data for BaM in this region. Note that force field calculations for Na-β (28) confirm that this region is dominated by the AlO_6 and Al_2O_7 groups. Thus it should be concluded that bands in the 512 to 614-cm^{-1} region correspond mainly to motions of octahedral polyhedra.

It is more difficult to confirm the assignment of the modes of E_{1g} and E_{2g} symmetry. Nevertheless, there is a striking agreement between the highest mode observed for α-Fe_2O_3 at 613 cm^{-1} (E_g symmetry) and the E_{1g}–E_{2g} doublet observed in BaM at about the same frequency. Therefore this doublet might be assigned to motions of the octahedra. To confirm the assignment of this mode, we use the mass ratio argumentation as above for the corresponding 815 (E_{1g}) and 816-cm^{-1} (E_{2g}) modes of Na-ß. Dohy *et al.* (28) interpret this doublet as modes involving an equal participation of Al and O atoms in an octahedron. The found ratio $\nu_{BaM}/\nu_{Na\text{-}\beta} = 1.33$ confirms this interpretation and supports the octahedral hypothesis stated above. A more detailed analysis of the modes by using the experimental and calculated Raman spectra of Na-β is difficult, because of the lack of data for BaM. However, it is interesting to note that the same considerable lack has been observed for the Na-β spectra, where the problem has been solved by zone center calculations.

Two intense bands are only observed in the $X(YZ)\bar{X}$ Raman spectrum of BaM, the very narrow and intense E_{1g} bands at 173 and 184 cm^{-1}. A possible interpretation is to assign these bands to the motion of the spinel block as a whole. The arguments for this assignment are the following: Such modes are expected at low frequency, insensitive to localized effects, thus giving rise to narrow bands. For the spinel, either normal or inverse, no Raman mode is observed below 150 cm^{-1}, so the characteristic modes for the spinel block should be situated above this frequency. Note that this assignment cannot be obtained by mass ratio from Na-β (their spinel block motions are placed at 100–110 cm^{-1} (25, 28)). This situation is not surprising; a strict observation of the molecular modes, for which the mass ratio is a good approach, becomes less valid for low-frequency modes.

Modes involving the Ba^{2+} cation are expected at low frequency. The Ba^{2+} cations contribute one Raman-active (E_{2g}) and two IR-active ($A_{2u} + E_{1u}$) modes to the vibrational structure (see Table 1). Unfortunately, no Raman band could be detected below 150 cm^{-1}. Therefore, it is useful to discuss the BaM IR spectra reported in the literature. The IR spectra of BaM reported by Nicolic *et al.* (4, 5) exhibit three bands at low frequency: two bands of A_{2u} symmetry at 59 and 124 cm^{-1} and one band of E_{1u} symmetry at 95 cm^{-1}. Belotto *et al.* (7) found for BaM two low-frequency bands at 102 and 124 cm^{-1} and assigned both to vibrations of the Ba^{2+} cation. According to the earlier argumentation, we assign, in contrast, the mode of A_{2u} symmetry at 59 cm^{-1} to an in-plane movement of the cation and the mode of E_{1u} symmetry at 95 cm^{-1} to the out-of-plane movement of the cation. The intense A_{2u} band found at 124 cm^{-1} can be tentatively assigned to a motion of the spinel block as a whole.

It is reasonable to expect that the IR spectra of BaM obey the same frequency shift with respect to Na-β as observed for the BaM Raman spectra. Therefore, assuming, as for the Raman spectra, a frequency ratio of 1.25, the two highest Na-β IR modes (28) of A_{2u} symmetry at 916 and 869 cm^{-1} shift to $\sim$720 and $\sim$690 cm^{-1}, respectively. In the reported IR spectra (4–7) no band has been observed at 720 cm^{-1}. On the other hand, a very strong and broad band in the region of 690 cm^{-1} can be observed. We assume that the expected band at 720 cm^{-1} is weak and masked by the strong band at 690 cm^{-1}. This is in striking corresponding with what has been observed for the high-frequency Raman spectra.

Another interesting point concerning the IR data of Nicolic *et al.* (4, 5) is the observed splitting of TO- and LO-frequency for a given mode. In general, the magnitude of the splitting gives an approximated order of the degree of ionicities. For comparison, spinels are mainly ionic while some of them reveal a certain amount of covalency (49). For the IR spectra of BaM an important splitting of the TO- and LO-frequency is observed and therefore the degree of ionicities should be relatively high, which is in agreement with the expected ionic character of the Fe–O bonds.

FIG. 4. (I) Schematic comparison of Na-β and BaM Raman spectra. (IIa) Interpretation of the frequency ratio for Na-β and BaM: type of atomic motions. (IIb) Energy level diagram describing the correlation of A_{1g} modes of Na-β and BaM. (III) Schematic spectra of ferrites where the highest modes are octahedra dominated. Schematic spectra of ferrites where the highest modes are tetrahedra dominated.

[a] Full lines, A_{1g} modes; interrupted lines, E_{1g} modes; dotted lines, E_{2g} modes.

[b] Only A_{1g} modes are represented.

[c] Full lines, A_{1g} modes; interrupted lines, E_g modes; dotted lines, T_{2g} modes.

[d] Assignment reported in ref 28.

[e] Assignment for A_{1g} modes.

[f] No symmetry assignment was reported in ref 20.

B. Thermal effects

It is of interest to study the temperature effects on the frequencies, intensities, and line widths of the normal modes of BaM (Fig. 3). As expected, the frequencies of the BaM Raman and IR spectra generally decrease with increasing temperature T, whereas the line widths $\Gamma_{1/2}$ increase with T. This is due to anharmonicity, as can be shown by perturbation theory (50).

1. Disorder. It is well known that X-ray or neutron diffraction does not furnish valuable information about the temporal behavior of the atoms. The same atomic positions and thermal parameters would be obtained for a single atom presenting either a dynamic or static disorder. Raman spectroscopy instead, like Mössbauer spectroscopy, can give valuable information about the dynamic behavior of the atoms.

As already mentioned, the mirror plane position of the trigonal iron atom in BaM might be only the average position of a static or dynamic disorder on this site. The study of the temperature-dependent evolution of the frequency, the number of observed bands, and the line width $\Gamma_{1/2}$ in Raman and IR spectra should shed more light on the nature of this disorder.

In the following we will describe the expected behavior in the form of three scenarios which might be considered:

(a) The equilibrium position is in the mirror plane but the associated potential is rather flat: For this case the selection rules in Table 1 are obeyed. However, the $\Gamma_{1/2}$ of the bipyramid-related bands can be important even below room temperature, due to possible large thermal motions along the c-axis.

(b) Dynamic disorder due to hopping in a double-well potential: the same irreducible representation can be considered. The bands associated with iron atoms in the trigonal site are expected to be broad at room temperature. When the temperature decreases, $\Gamma_{1/2}$ is expected to decrease considerably, if an ordering takes place (see Section III.B). Assuming a complete ordering at lower temperature, the irreducible representation of Table 1 is no longer respected and an increase of bands is expected.

(c) Static disorder at room temperature with a statistical distribution of the $Fe^{(2)}$: In such a case selection rules can be relaxed and the bands associated with the bipyramidal site are expected to be broad at any temperature.

The line widths $\Gamma_{1/2}$ of the bands in the Raman spectra at room temperature and moreover at 80 K are not compatible with a high rate of a static disorder. Thus we rule out case c. The number of bands at room temperature is compatible with both model a and model b. However, when the temperature is decreased, no extra bands are observed, which would explain the appearance of a superstructure due to ordering of the $Fe^{(2)}$ ions. Thus, the number of bands and their $\Gamma_{1/2}$ reduction when the temperature is decreased favors model a or model b with a potential barrier lower than 80 K. The foregoing discussion is strengthened by the BaM IR spectra at 80 and 300 K of Nicolic *et al.* (5).

The bandwidth of the A_{1g} mode at 684 cm^{-1} is more than halved when going from 300 to 80 K (Fig. 3), whereas the widths of the other modes decrease less dramatically. This particular behavior is in good agreement with the expected scenarios a and b for the bipyramid-associated band. It is important to note that the thermal behavior of this band strengthens its assignment given in Section V.A.3.

Marshall and Sokoloff (8) proposed on the basis of their phonon spectral calculation a new hypothetical scenario for the temperature dependence of the trigonal site (see Section III.1). In particular, they predicted a soft-mode behavior for the lowest transverse optic mode at $\sim$111 cm^{-1} associated with the vibration of the iron ions along the c-axis. This mode is of A_{2u} symmetry and is expected to be IR active. Actually, no drastic changes are observed in the BaM IR spectra between 300 and 80 K and there are no data below 80 K. Furthermore, no frequency is observed below 50 cm^{-1} although the IR spectrum has been recorded down to 20 cm^{-1}. Therefore, the soft-mode behavior remains to be clarified by further low-temperature and low-frequency IR spectra.

2. Magnons. In addition to the vibrational bands, Raman spectra of magnetic solids have bands due to collective magnetic excitations known as quantified spin waves or magnons (51). For magnetic Raman scattering the frequency shifts are typically smaller (<100 cm^{-1}). However, for magnetite (Fe_3O_4) Hart *et al.* (46) observed a Raman band due to one-magnon scattering at 472 cm^{-1}; this observation has been confirmed by Degiorgi *et al.* (18). For BaM only the Fe^{3+} ions have a magnetic moment, each with spin $\frac{5}{2}$. Their moments order ferrimagnetically below $T_C = 723$ K. There are two formula units within each hexagonal unit cell, which leads to 24 distinct crystallographic sites and thus 24 spin wave modes. Marshall and Sokoloff (9) calculated the spin wave spectra for BaM in anticipation of a detailed analysis of the ferrimagnetic resonance relaxation. According to these authors, BaM spin waves should be observed in the 0- to 600-cm^{-1} region. Therefore, in addition to the phonon lines, additional lines might be observed in the BaM Raman spectra which are related to one-magnon scattering from a spin wave optic branch.

Magnetic Raman scattering is typically weaker than vibrational scattering and in particular sensitive to temperature effects. In the Raman spectra of BaM no band that might be associated with magnon scattering is observed. On this basis, all the bands of the BaM Raman spectra can be assigned to vibrational modes. However, some very weak peculiarities in the expected region are observed in the 80 K spectra, but for their unambiguous identification, additional

experiments, especially at very low temperature, are required.

VI. CONCLUSION

Raman spectra of BaM at 80 K and room temperature have been obtained for the first time. Of the 42 Raman-active modes 33 have been observed; the spectra have been assigned in terms of symmetry.

By comparison with similar compounds (β-alumina and much simpler ferrites) and by using rules governing the frequency evolution versus the coordination number and the degree of connection, it has been possible to attribute the stretching modes of characteristic groups of atoms. In particular, the symmetric stretching mode of the bipyramidal $Fe^{(2)}O_5$ group, characteristic of the M-hexaferrite structure, has been found to be responsible for the strongest Raman band at 684 cm^{-1}. The evolution of this band with temperature has led us to conclude that the $Fe^{(2)}$ atom is dynamically disordered at room temperature and that from the vibrational spectroscopic point of view, the data can be interpreted as if the ion was moving in a single potential well. We cannot exclude the possibility of having a double well; in such a case the potential barrier would be lower than 80 K. Our observation is in agreement with a possible transition from a very shallow double well at higher temperatures to a local minimum in the mirror plane at lower temperatures, which was up to now only a speculative prediction based on a phonon spectral calculation by Marshall and Sokoloff (8). However, their predicted soft-mode behavior of the lowest TO-optic mode could not be detected. Therefore, the consequences of the suggested soft mode deserve further experimental attention, especially light scattering experiments at low temperature.

The detailed study of Ir–Co-substituted crystals and thin films will be treated in a subsequent publication.

REFERENCES

1. P. B. Braun, *Philips Res. Rep.* **12,** 491 (1957).
2. J. Smit and H. P. J. Wijn, in "Ferrites" (M. J. F. Marchand, Ed.), pp. 193–228. Philips Technical Library, Eindhoven, 1961.
3. W. Buchner, R. Schliebs, G. Winter, and K. H. Buchel, "Industrial Inorganic Chemistry." VCH, Weinheim, 1989.
4. P. M. Nicolic, L. Zivanov, O. S. Aleksic, D. Samaras, G. A. Gledhill, and J. D. Collins, *Infrared Phys.* **30,** 265 (1990).
5. P. M. Nicolic, M. B. Pvlovic, Z. Maricic, S. Duric, Lj. Zivanov, D. Samaras, and G. A. Gledhill, *Infrared Phys.* **33,** 401 (1992).
6. A. Eremenko, Y. Pashkevich, V. Pishko, and V. Tsapenko, *Physica B* **194,** 189 (1994).
7. M. Belotto, G. Busca, C. Cristiani, and G. Groppi, *J. Solid State Chem.* **117,** 8 (1995).
8. S. P. Marshall and J. B. Sokoloff, *Phys. Rev. B* **44,** 619 (1991).
9. S. P. Marshall and J. B. Sokoloff, *J. Appl. Phys.* **67,** 2017 (1990).
10. R. D. Waldron, *Phys. Rev.* **99,** 1727 (1955).
11. P. Tarte, *Spectrochim. Acta*, *Part A* **23,** 2127 (1967).
12. J. Preudhomme and P. Tarte, *Spectrochim. Acta*, *Part A* **27,** 845 (1971).
13. J. Preudhomme and P. Tarte, *Spectrochim. Acta*, *Part A* **27,** 1817 (1971).
14. S. Onari, T. Arai, and K. Kudo, *Phys. Rev. B* **16,** 1717 (1977).
15. H. D. Lutz, B. Müller, and H. J. Steiner, *J. Solid State Chem.* **90,** 54 (1991).
16. K. F. McCarty and D. R. Boehme, *J. Solid State Chem.* **79,** 19 (1989).
17. P. R. Graves, C. Johnson, and J. J. Campaniello, *Mater. Res. Bull.* **23,** 1651 (1988).
18. L. Degiorgi, I. Blatter-Mörke, and P. Walter, *Phys. Rev. B* **35,** 5421 (1987).
19. K. F. McCarty, J. Z. Liu, R. N. Shelton, and H. B. Radousky, *Phys. Rev. B* **31,** 8792 (1990).
20. M. I. Baraton, G. Busca, V. Lorenzelli, and R. J. Willey, *J. Mater. Sci. Lett.* **13,** 275 (1994).
21. S. Venugopalan, M. Dutto, A. K. Ramdas, and J. P. Remeika, *Phys. Rev. B* **31,** 1490 (1985).
22. S. Venugopalan, M. Dutto, A. K. Ramdas, and J. P. Remeika, *Phys. Rev. B* **27,** 3115 (1983).
23. N. Koshizuka and S. Ushioda, *Phys. Rev. B* **22,** 5394 (1980).
24. C. Thomsen, R. Wegerer, H. U. Habermeier, and M. Cardona, *Solid State Commun.* **83,** 199 (1992).
25. C. H. Hao, L. L. Chase, and G. D. Mahan, *Phys. Rev. B* **13,** 4306 (1976).
26. Ph. Colomban and G. Lucazeau, *J. Chem. Phys.* **72,** 1213 (1980).
27. G. Lucazeau, *Solid State Ionics* **8,** 1 (1983).
28. D. Dohy, G. Lucazeau, and D. Bougeard, *Solid State Ionics* **11,** 1 (1983).
29. R. Frech and J. B. Bates, *Spectrochim. Acta. Part A* **35,** 685 (1979).
30. S. Pignard, J. P. Sénateur, H. Vincent, J. Kreisel, and A. Abrutis, *J. Phys IV* **7,** 483 (1997).
31. B. Sugg and H. Vincent, *J. Magn. Magn. Mater.* **139,** 364 (1995).
32. H. Vincent, E. Brando, and B. Sugg, *J. Solid State Chem.* **120,** 17 (1995).
33. J. P. Sénateur, F. Weiss, O. Thomas, R. Madar, and A. Abrutis, French Patent No. 93/08838, PCT No. FR94/00858.
34. J. G. Rensen and J. S. van Wieringen, *Solid State Commun.* **7,** 1139 (1969).
35. X. Obradors, A. Collomb, M. Pernet, D. Samaras, and J. C. Joubert, *J. Solid State Chem.* **56,** 171 (1985).
36. X. Obradors, X. Solans, A. Collomb, D. Samaras, J. Rodriguez, M. Pernet, and M. Font-Altaba, *J. Solid State Chem.* **72,** 218 (1988).
37. A. Collomb, P. Wolfers, and X. Obradors, *J. Magn. Magn. Mater.* **62,** 57 (1986).
38. E. Kreber, U. Gonser, and A. Trautwein, *J. Phys. Chem. Solids* **36,** 263 (1975).
39. A. Trautwein, E. Kreber, U. Gonser, and F. E. Harris, *J. Phys. Chem. Solids* **36,** 325 (1975).
40. V. Adelsköld, *Min. Geol.* **12A**, 1 (1938).
41. V. D. Townes, J. H. Fang, and A. S. Perrotta, *Z. Kristallogr.* **125,** 437 (1967).
42. W. G. Fately, N. N. McDevitt, and F. F. Bentley, *Appl. Spectrosc.* **25,** 155 (1971).
43. S. Bhagavantam and T. Venkatarayudu, *Proc. Indian Acad. Sci., Sect. A* **9,** 224 (1939).
44. W. B. White and B. A. DeAngelis, *Spectrochim. Acta*, *Part A* **23,** 985 (1967).
45. T. R. Hart, S. B. Adams, and H. Temkin, *in* "Light Scattering in Solids" (M. Balkanski, R. C. C. Leite, and S. P. S. Porto, Eds.), p. 259, Wiley, New York, 1975.
46. T. R. Hart, H. Temkin, and S. B. Adams, *in* "Light Scattering in Solids" (M. Balkanski, R. C. C. Leite, and S. P. S. Porto, Eds.), p. 254. Wiley, New York, 1975.
47. H. Shirai, Y. Morioka, and I. Nakagawa, *J. Phys. Soc. Jpn.* **51,** 592 (1982).
48. S. P. S. Porto and S. Krishnan, *J. Chem. Phys.* **47,** 1009 (1967).
49. J. Zwinscher and H. D. Lutz, *J. Alloys Compd.* **219,** 103 (1995).
50. M. Balkanski, R. F. Wallis, and E. Haro, *Phys. Rev. B* **28,** 1928 (1983).
51. A. K. Ramdas and S. Rodriguez, *in* "Light Scattering in Solids VI" (M. Cardona and G. Güntherodt, Eds.), Chap. 4. Springer, Berlin, 1991.